

An Analysis of Roping in AA6016 Sheet by Through-thickness Texture Measurements and Numerical Simulations

A. Guillotin^{1,2}, G. Guiglionda², C. Maurice¹ and J.H. Driver¹

¹ Ecole Nationale Supérieure des Mines de Saint-Etienne, 158 cours Fauriel, 42023 Saint Etienne, France

² Alcan Centre de Recherches de Voreppe, 725 rue Aristide Bergès, BP 27, 38341 Voreppe cedex, France

The origins of strain-induced surface roughness in three AA6016-T4 sheets has been studied. Each sheet, as a result of different processing routes, exhibits different roping intensities after stretching (A=high, B=low, and C=no-roping). A detailed analysis of the microtexture variation through the sheets was carried out in 3D by acquiring a series of 2D EBSD scans from the surface to the mid-thickness. The step size, in the through-thickness direction, was chosen to be about the grain size, given the macroscopic scale of the roping phenomenon. The measured texture layers were then used as input for 3D idealized Crystal Plasticity Finite-Element simulations (CPFEM).

The results show that texture banding/clustering along RD is present in the very first surface layers and that this spatial banding is quite different from one grain layer to another. In sheet A, the Cube/Goss orientations are distributed in near-alternating fashion. Cube/ND-rotated-Cube and Cube/Random form, respectively, the banded structures of sheets B and C. CPFEM demonstrates that the mechanical behavior of these pairs of textures is sufficient to promote strain heterogeneity when layers are unconstrained. But when they are embedded within a 3D homogeneous medium, the out-of plane strain heterogeneity of the banded layers is significantly reduced. By comparing the surface roughness morphology after stretching with the through-thickness texture distribution, and allowing for the decreasing mechanical influence of grain layers with depth, it is shown that the out-of plane strain of the first 4 or 5 surface grains layers plays an important role in roping of AA6016 sheets.

Keywords: Al-Mg-Si aluminium alloy, roping, through-thickness texture, CPFEM.

1. Introduction

Energy consumption in the transportation sector could be significantly decreased by weight reduction. The Al-Mg-Si alloys such as AA6016 are suitable for this purpose but, during forming operations, can sometimes be prone to roping, a well-known surface roughening defect. Roping is characterized by visible lines (several centimeters) along the rolling direction (RD) when the sheet is plastically stretched in the transverse direction (TD). This alternating distribution of ridges and valleys limits their use for outer panel applications for cosmetic reasons. Despite much work a better understanding of the relationship between microstructure and roughness morphology is still needed.

As the spatial distribution of texture is claimed to be a predominant factor, e.g. [1], EBSD has been widely used in the analysis of strain-induced surface roughness [1-8]. It has already been shown that a high roping level is often associated with the alignment of clustered crystallographic components such as $\{100\}\langle 001\rangle$ Cube and $\{110\}\langle 001\rangle$ Goss. By crystal plasticity modeling, Cube and Goss show different mechanical behaviors that can explain, in a given grain layer, the anisotropic development of roping. However, three-dimensional texture distributions are required to have a more general view of the mechanical phenomenon and possible interactions between the grain layers.

2. Methods

2.1 Materials and Roping Test

Three different AA6016-T4 sheets with the same chemical composition were used in this study. They were produced to 1mm sheet using different processing routes and denoted A, B and C. In order

to determine the surface appearance after deformation, 50(RD)x200(TD)mm² samples of each sheet were stretched 15% along TD, and carefully stoned. This gives a visual assessment of the roping level which depends on the macroscopic surface morphology.

2.2 Experimental Investigation

The through-thickness texture investigation was achieved by serial sectioning and EBSD measurements. From the surface to the mid-thickness, the microtextures of the three materials were determined grain layer by grain layer on 7x14mm² areas. Indentation marks gave an accurate localization of section positions.

EBSD scans were performed in a JEOL 6500F equipped with an HKL Technology system. The acquisition parameters were set to 20kV for the accelerating voltage, 18.1mm for the working distance, 70° for the tilt angle, 8x8 binning, 1 frame per point, Hough resolution at 65, and magnification to 300. The EBSD step size was taken as 6μm to reveal the grain structure.

Controlled sectioning of the (RD,TD) planes was carried out by electropolishing using a commercial A2 Struers solution and LectroPol-5 Struers machine. The experimental dissolution rate had been carefully calibrated to 0.2μm/s with 22V applied on 20mm² active surface. So, with a 150s hold-time, 30μm of material was removed and checked by manual micrometer after the EBSD scan.

2.3 Numerical Model and Meshes

To incorporate grain interactions as required for texture clustering effects, a three-dimensional Crystal Plasticity Finite-Element Method (CPFEM) has been used to simulate strain-induced surface roughness. Elastic deformations were neglected, and mechanical equilibrium was attained at the end of each time-step by three levels of iteration. More details of the CPFEM model can be found in [10].

The code employed a rate-dependant crystal plasticity relation in order to determine the slip rates on the 12 fcc crystal slip systems of {111} planes and <110> directions. The strain-rate sensitivity exponent was set as low as possible (m=0.05) in order to reproduce room temperature behavior and to avoid numerical convergence issues.

Isotropic hardening was assumed by a modified Voce law (Equation 1). Here Θ_0 is the initial hardening rate, Θ_{IV} is the stage IV hardening rate and τ_s is the saturation resolved shear stress. The parameter values of Table 1 were determined by fitting to experimental loading tests.

$$\Theta = \Theta_{IV} + \Theta_0 \left(\left| 1 - \frac{\tau}{\tau_s} \right|^\alpha \text{sign} \left(1 - \frac{\tau}{\tau_s} \right) \right) \quad (1)$$

Table 1: Fitting parameters used in the CPFEM hardening law

Parameters	Θ_0	Θ_{IV}	τ_s	α
Fitted values	1900MPa	11MPa	273MPa	9

Two kinds of idealized meshes, respectively denoted thin (77x77x1 elements) and thick (34x34x5 elements), were built (Figure 1), both limited to 6000 cubic elements (20 nodes and 8 integration points each) for reasonable calculation times. A single crystallographic orientation was assigned per element, and each mesh contained a layer composed of a matrix zone around a banded zone (10 elements in width) in order to artificially reproduce experimental texture clusters. Mesh deformation was imposed by assigning boundary displacement to nodes located on the free surfaces of the RD/TD planes. Uniaxial tensile straining was simulated by 60 increments of 0.0025 logarithmic strains along TD, and of -0.00125 along RD.

The simulated roughness of the top surface was expressed in terms of the height differences Δh between the current point and the mid-plane. This distance was converted into μm by assuming that the element size was equal to the average grain size (30μm). Moreover, variation profiles along TD

were calculated and plotted by averaging all the values with the same coordinates along RD in order to highlight the roughness alignment.

In addition to this computer intensive CPFEM model, we have also set up a faster and more flexible model which could work directly from EBSD texture maps. This model was inspired by the SRM model described by [11], and simulated the individual out-of plane strains from crystallographic orientations. A preliminary study, not presented here, led to the same conclusion concerning its ability to give reliable indicators for qualitative roughness characterization.

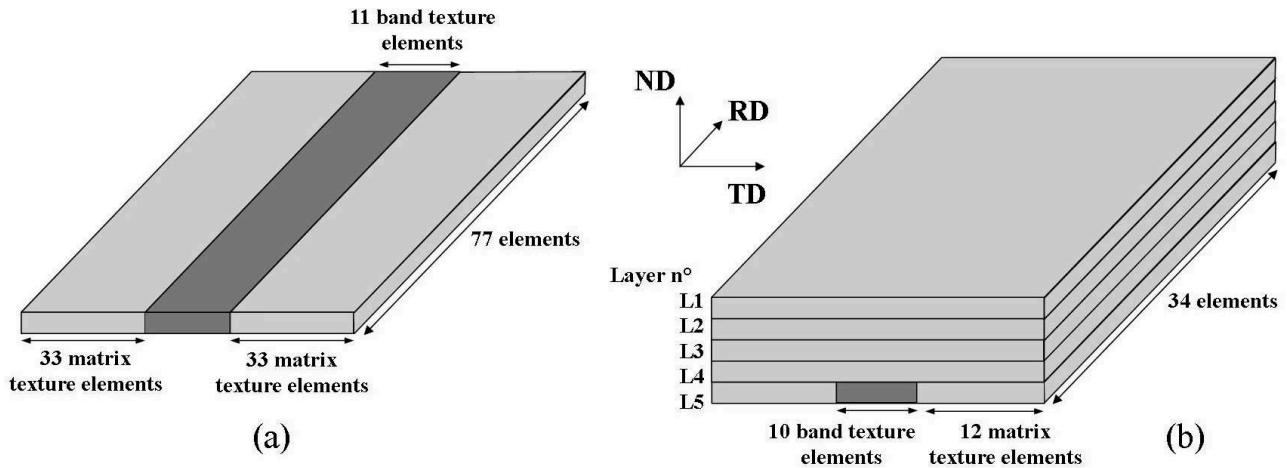


Figure 1: CPFEM mesh configurations: (a) = Thin mesh (b) = Thick mesh

3. Results and Discussion

3.1 Surface Roping Levels

Figure 2 shows the surface appearance of the three materials after tensile deformation. A regular and strong pattern aligned along RD is present on the surface of sample A revealing a high roping level. Sample B reveals a weaker banded structure caused by a lower density of peaks and valleys, resulting in a lower roping intensity. Sample C is practically roping-free since its surface roughness is more isotropic and randomly distributed.



Figure 2: Surface roughness stoned pictures of materials after 15% stretching along TD: (a) = Sheet A (high roping level) (b) = Sheet B (low roping level) (c) = Sheet C (roping free)

3.2 Through-thickness Texture Measurements

The texture of the first surface layer is very weak, and its spatial distribution is almost random.

But, further down, EBSD maps showed that texture clustering is present through all the thickness sections, from the second grain layer to the central one as also observed by [5,8]. Moreover, the spatial localization of features and texture intensity changed from one layer to another.

The average grain size measured from EBSD maps of all three sheets is very fine for the first grain layers, but attained a maximum in layers located between 55 μ m and 115 μ m under the surface as can be seen in Figure 3. In the literature, many investigations have shown that the orange peel surface, as characterized by the standard R_a parameter, is proportional to the average grain size (see e.g. [12,13]).

Although grain size evolution is limited in our materials, it is legitimate to assume that bigger grain size layers could have more mechanical influence on roughness development than other layers.

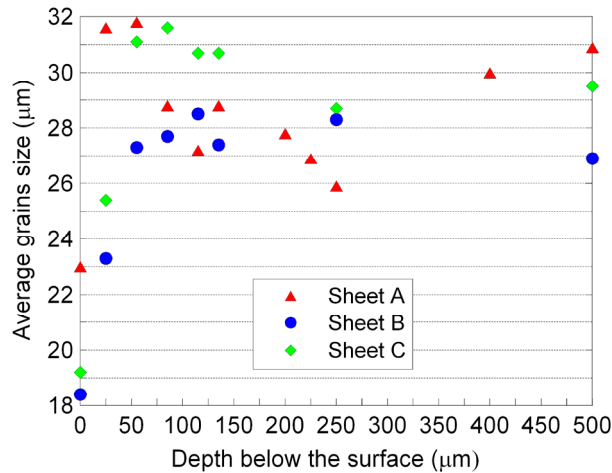


Figure 3: Average grain size as a function of depth

It is noteworthy that the texture intensity follows the same trend as the average grain size and exhibits a peak at around 55μm beneath the surface. Figure 4 shows out-of plane strain maps calculated from experimental EBSD measurements (55μm depth) by the SRM model, and ODF sections ($\varphi_2=0^\circ$) of some selected areas.

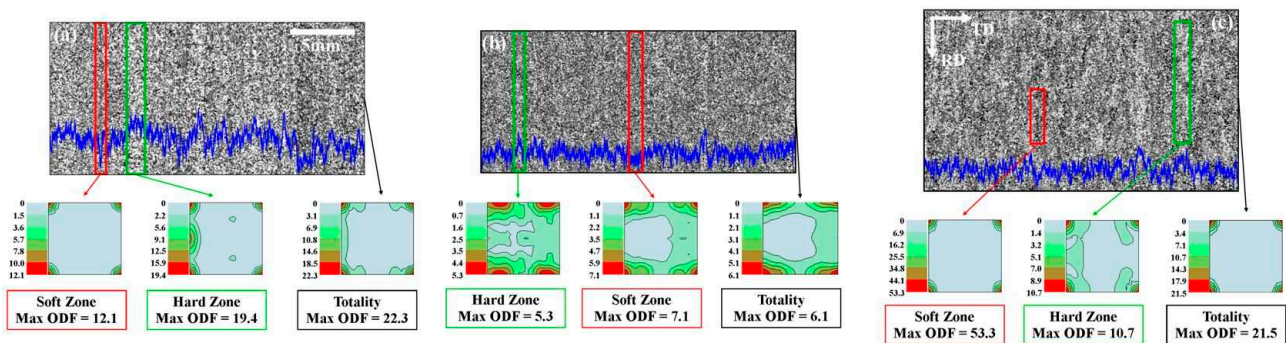


Figure 4: Simulated out-of plane strains of grain layers located at 55μm beneath the surface.

ODF sections ($\varphi_2=0^\circ$) of Hard and Soft selected Zones are shown.

(a) = Sheet A (high roping level) (b) = Sheet B (low roping level) (c) = Sheet C (roping free)

In each material, the Cube component is the preferred orientation but its intensity was not directly correlated to the roping level (intensities about 20x for sheets A and C, but about 6x for sheet B). Paired with Cube, another minority texture component is usually present. Sheet A is composed of a significant alignment along RD of Cube and Goss. The microtexture of sheet B could be seen as a Cube matrix grooved by few ND-rotated-Cube bands, giving a more diffused and homogeneous pattern. Finally, sheet C reveals a chaotic and unordered distribution of strong Cube clusters in a more Random texture background. The size of the Cube clusters was of the same order as the observed roughness features.

3.3 Mechanical Behavior

The above texture pairs were employed as input data to build the idealized meshes and for several deformation simulations. The roughness results obtained on the thin meshes stretched along TD are presented in Figure 5. It turns out that for a TD stretch all the selected pairs of texture have different mechanical responses that are sufficient to generate a macroscopically organized roughness, i.e. not

only the Cube/Goss pair [1,7,14,]. Therefore, an explication of the three different roping levels in these materials does not only depend on the different texture pairs as identified here.



Figure 5: Simulated surface roughness profiles for the three materials for a stretch along TD. These results were obtained by CPFEM on one element thickness meshes. The red rectangles are the elements which contain a texture band. Units are in μm .

When a banded layer is embedded in a 3-dimensional medium, as shown in Figure 6, the roughness amplitude decreases gradually with the layer depth. When the banded layer is covered by 3 to 4 neutral layers, its influence on the surface can be regarded as negligible.

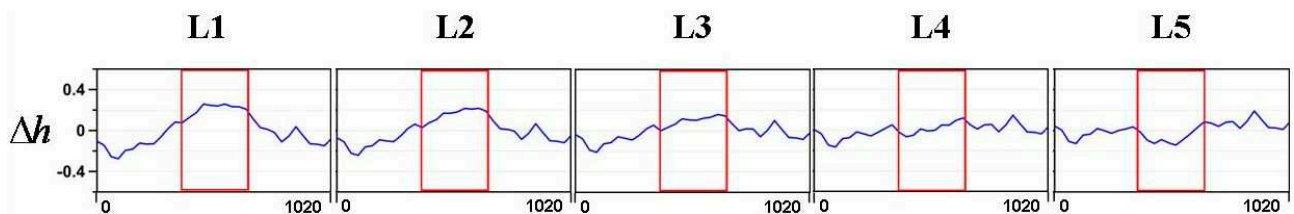


Figure 6: Simulated surface roughness profiles of material A for a thick mesh deformed by CPFEM. L1 refers to the mesh where the banded layer is located at the surface while L5 means that the banded layer is below 4 homogeneous grain layers. The red rectangles are the elements containing a texture band.

3.4 Wavelength Correlations Between Surface Roughness and Microstructural Features

A quantitative comparison between surface roughness morphology and microstructural features has also been achieved by frequency functions and correlation coefficient analysis. The method will be described elsewhere [15]. The microstructure of material A was selected for this study, since the width of the texture bands changed significantly through the sheet thickness.

The surface roughness of sheet A was described by its stoned picture (Figure 1(a)) which was resized because of distortion due to mechanical stretching, and re-sampled to fit the EBSD step size ($6\mu\text{m}$). Its spatial wavelengths have been determined by Areal Auto Correlation Function (AACF). At the same time, the AACF of each simulated out-of plane strains section (as maps presented in Figure 4) have also been calculated.

Finally, correlation coefficients were determined from spatial wavelengths of both surface roughness and simulated out-of-plane strain maps, and plotted against layer depth in Figure 7. The highest values were found for grain layers just below the sheet surface, and particularly for a depth of $55\mu\text{m}$. This means that the first 4 to 5 grains layers have a closer similarity to surface roughness than the other layers. It is a further argument to support the idea that these sub-surface layers lead to roping development.

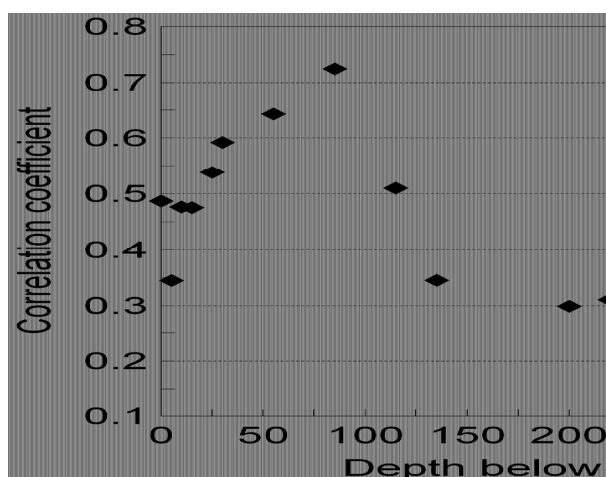


Figure 7: Wavelength correlation coefficients between surface roughness and microstructural features as a function of depth in material A.

Conclusions

In this work, the origin of roughness formation has been studied in three AA6016 sheets which exhibit different roping intensities after deformation. Experimental investigations in the through-thickness of the materials in addition to CPFEM simulations highlight the predominant contribution of the spatial distribution of texture of the first 4 to 5 grain layers in the development of strain-induced surface roughness. In particular, different texture pairs have been identified in the three sheets but their presence is insufficient to explain the roping levels.

Acknowledgement

The authors would like to thank Professor P. Bate for his support on FE modeling and for helpful discussions.

The support of the French "Fonds Unique Interministériel" and Conseil Général de la Loire to this part of the project "High formability automotive sheet for lightweight automotive" within the framework of the "Pôle de Compétitivité" ViaMéca is gratefully acknowledged.

References

- [1] P. D. Wu, D. J. Lloyd, A. Bosland, H. Jin and S. R. MacEwen: *Acta Mat.* 51 (2003) 1945-1957
- [2] A. Beaudoin, J. Bryant and D. Korzekwa: *Metal. Mat. Trans. A.* 29 (1998) 2323-2332
- [3] P.S. Lee, H.R. Piehler, B.L. Adams, G. Jarvis, H. Hampel and A.D. Rollett: *J. of Mat. Proc. Tech.* 80-81 (1998) 315-319
- [4] N.J. Wittridge and R.D. Knutsen: *Mat. Sci. Eng. A* 269 (1999) 205-216
- [5] G.J. Baczynski, R. Guzzo, M.D. Ball and D.J. Lloyd: *Acta Mat.* 48 (2000) 3361-3376
- [6] P.S. Lee, G. Jarvis, A.D. Rollett, H.R. Piehler and B.L. Adams: *Min. Met. Mat. Soc.* (2000) 161-169
- [7] D. Raabe, M. Sachtleber, H. Weiland, G. Scheele and Z. Zhao: *Acta Mat.* 51 (2003) 1539-1560
- [8] H. Jin, P.D. Wu, M.D. Ball and D.J. Lloyd: *Mater. Sci. Tech.* 4 (2005) 419-428
- [9] Y.S. Choi, A.D. Rollett and H.R. Piehler: *Mat. Trans.* 47 (2006) 1313-1316
- [10] P. S. Bate: *Phil. Trans. R. Soc. Lond. A.* 357 (1999) 1589-1601
- [11] P. D. Wu, D. J. Lloyd and S. R. MacEwen: *Scr. Mat.* 48 (2003) 1243-1248
- [12] M.R. Stoudt and R. Ricker: *Metal. Mat. Trans. A* 33 (2002) 2883-2889
- [13] Y.Z. Dai and F.P. Chiang: *J. of Eng. Mat. Tech.* 114 (1992) 432-438
- [14] Z. Zhao, R. Radovitzky and A. Cuitino: *Acta Mat.* 52 (2004) 5791-5804
- [15] A. Guillotin, G. Guiglionda, C. Maurice and J.H. Driver: to be published